

# A compact fiber optics-based heterodyne combined normal and transverse displacement interferometer

Bryan Zuanetti, Tianxue Wang, and Vikas Prakash

Citation: [Review of Scientific Instruments](#) **88**, 033108 (2017); doi: 10.1063/1.4978340

View online: <https://doi.org/10.1063/1.4978340>

View Table of Contents: <http://aip.scitation.org/toc/rsi/88/3>

Published by the [American Institute of Physics](#)

---

## Articles you may be interested in

[Fast, precise, and widely tunable frequency control of an optical parametric oscillator referenced to a frequency comb](#)

[Review of Scientific Instruments](#) **88**, 033101 (2017); 10.1063/1.4977049

[High stable remote photoelectric receiver for interferometry](#)

[Review of Scientific Instruments](#) **88**, 033105 (2017); 10.1063/1.4978341

[A heterodyne straightness and displacement measuring interferometer with laser beam drift compensation for long-travel linear stage metrology](#)

[Review of Scientific Instruments](#) **88**, 035114 (2017); 10.1063/1.4978802

[A compact atomic beam based system for Doppler-free laser spectroscopy of strontium atoms](#)

[Review of Scientific Instruments](#) **88**, 033103 (2017); 10.1063/1.4977593

[Invited Review Article: Tip modification methods for tip-enhanced Raman spectroscopy \(TERS\) and colloidal probe technique: A 10 year update \(2006-2016\) review](#)

[Review of Scientific Instruments](#) **88**, 031101 (2017); 10.1063/1.4978929

[High resolution and stability roll angle measurement method for precision linear displacement stages](#)

[Review of Scientific Instruments](#) **88**, 023102 (2017); 10.1063/1.4974816

---

PHYSICS TODAY

WHITEPAPERS

## MANAGER'S GUIDE

Accelerate R&D with  
Multiphysics Simulation

READ NOW

PRESENTED BY

 COMSOL

# A compact fiber optics-based heterodyne combined normal and transverse displacement interferometer

Bryan Zuanetti, Tianxue Wang, and Vikas Prakash<sup>a)</sup>

*Department of Mechanical and Aerospace Engineering, Case Western Reserve University, Cleveland, Ohio 44106, USA*

(Received 20 December 2016; accepted 26 February 2017; published online 21 March 2017)

While Photonic Doppler Velocimetry (PDV) has become a common diagnostic tool for the measurement of normal component of particle motion in shock wave experiments, this technique has not yet been modified for the measurement of combined normal and transverse motion, as needed in oblique plate impact experiments. In this paper, we discuss the design and implementation of a compact fiber-optics-based heterodyne combined normal and transverse displacement interferometer. Like the standard PDV, this diagnostic tool is assembled using commercially available telecommunications hardware and uses a 1550 nm wavelength 2 W fiber-coupled laser, an optical focuser, and single mode fibers to transport light to and from the target. Two additional optical probes capture first-order beams diffracted from a reflective grating at the target free-surface and deliver the beams past circulators and a coupler where the signal is combined to form a beat frequency. The combined signal is then digitized and analyzed to determine the transverse component of the particle motion. The maximum normal velocity that can be measured by this system is limited by the equivalent transmission bandwidth (3.795 GHz) of the combined detector, amplifier, and digitizer and is estimated to be  $\sim 2.9$  km/s. Sample symmetric oblique plate-impact experiments are performed to demonstrate the capability of this diagnostic tool in the measurement of the combined normal and transverse displacement particle motion. *Published by AIP Publishing.* [<http://dx.doi.org/10.1063/1.4978340>]

## I. INTRODUCTION

Optical interferometry has become one of the most widely used diagnostic tools for shockwave experiments. Over the years, the conventional Normal Displacement Interferometer (NDI),<sup>1–5</sup> the Velocity Interferometer System for Any Reflector (VISAR),<sup>6,7</sup> and more recently, the Photonic Doppler Velocimeter (PDV)<sup>8,9</sup> have become some of the well accepted non-contact optical methods to measure the normal component of the free surface particle motion in shock wave experiments.

In the case of oblique plate-impact experiments, it is vital to monitor the combined motion of the free surface of the target plate resulting from the generation of both longitudinal and transverse waves at impact. In this regard, the normal and transverse displacement interferometer (NDI/TDI)<sup>10,11</sup> uses an array of mirrors and related optics along with a high frequency holographic diffraction grating to record fringes related to the normal and transverse motion of the free surface of the target plate. Other researchers have utilized the shear wave velocity interferometer<sup>12–15</sup> that involves the use of two VISAR channels to measure particle velocity motion along two beams diffracted off the same point on a diffuse target to obtain the combined normal and transverse particle velocity history.

Recent studies by Dolan<sup>16</sup> and Wu *et al.*<sup>17</sup> have shown that an all fiber-optics-based PDV is inexpensive, compact, and yet a robust system which can be applicable wherever the VISAR can be used. The system is relatively simple to assemble and requires little calibration post assembly, making it less

time consuming to use with respect to the conventional displacement interferometry techniques. Moreover, fiber-coupled components enable the PDV to be robust and insensitive to experimental variation.<sup>18</sup> Conventional optical components such as those used in the NDI/TDI may result in low fringe contrast if proper care is not taken to prevent misalignment.<sup>19</sup> These components are also sensitive to rotation of the target reflective surface due to non-planar impact and the relatively long optical legs used in conventional interferometry setups.<sup>18</sup> PDV is able to measure a broad range of particle velocities (several m/s up to km/s), with high accuracy ( $\pm 0.1\%$ ) which is comparable to or even superior to that of a VISAR.<sup>20</sup> Additionally, the 1550 nm wavelength laser source used in PDV, in contrast to the visible light used in other interferometry techniques, results in a lower beat frequency and enables the use of lower frequency digitizers than required for the conventional NDI/TDI or VISAR.<sup>8</sup>

The present paper describes the design and implementation of a compact all fiber-optic-based heterodyne displacement interferometer to measure the combined normal and transverse displacement particle motion of the free surface of the target plate. This fiber-optics-based interferometer has many of the advantages of both the conventional NDI/TDI and VISAR, while avoiding major disadvantages of the individual systems such as set-up time, cost, maintenance, and size. A brief description of the conventional PDV and the combined normal and transverse displacement interferometer is provided in Section II. Section III presents the design and implementation of the new all-fiber-optic-based NDI/TDI developed in the present study, followed by an analysis of the performance and performance-limits of the system. Finally, experimental data

<sup>a)</sup> Author to whom correspondence should be addressed. Electronic mail: [vikas.prakash@case.edu](mailto:vikas.prakash@case.edu)

and results from a series of two symmetric oblique plate impact experiments are presented in Section IV, to demonstrate the ability of the new fiber-optic-based combined NDI/TDI.

## II. BACKGROUND

### A. The conventional photonic Doppler velocimeter (PDV)

The conventional PDV, also known as heterodyne velocimetry, is fundamentally a fiber-based Michelson interferometer. In essence, the technique involves combining a reference beam with a Doppler shifted beam to create beat frequency variations, which are analyzed to obtain the particle velocity time-history of a point in shock-wave experiments. The original PDV, developed by Strand *et al.*,<sup>8</sup> was built using off-the-shelf components used by the telecommunication industry; this design is shown schematically in Fig. 1. A 1550 nm fiber laser is used to illuminate the target, and single mode fibers are chosen to transport the laser light through each component of the system. The interferometer also makes use of an optical component called a three-port circulator. The circulator allows light emitted from Port 1 to exit from Port 2 and light from Port 2 to exit from Port 3 while preventing back reflection. Using these three main optical components, the system functions as follows: laser-light from a fiber-coupled laser is made to pass through a circulator onto a focusing probe via single mode optical fibers. The probe serves as both a source and collector of light and directs the laser beam onto a point on the target surface. The Doppler shifted light from the target surface is transported back into the optical fiber; the beam enters the circulator through Port 2 and leaves the circulator through Port 3, where they are combined to form a beat signal, attenuated, and then sent to the detector.

The resultant time dependent intensity,  $I(t)$ , measured by the detector is given by<sup>8</sup>

$$I(t) = I_o + I_d + \sqrt{I_o I_d} \sin [f_b(t) + \varphi], \quad (1)$$

where  $I_o$  and  $I_d$  are the intensities of the non-Doppler shifted light and Doppler shifted light, respectively, and  $\varphi$  is the relative phase between the two. The frequency of the beat signal

$f_b(t)$  is given by the absolute difference between the reference and Doppler shifted (target) beams and can be expressed as

$$f_b(t) = 2 \left[ \frac{v_n(t)}{c} \right] f_o, \quad (2)$$

where  $v_n(t)$  is the normal velocity of the target reflective surface, and  $c$  is the speed of light. Using the relationship between the speed and wavelength of light, Equation (2) can be written as

$$v_n(t) = \frac{\lambda_o}{2} f_b(t), \quad (3)$$

where  $\lambda_o$  is the wavelength of the fiber laser. Equation (3) is used to determine the velocity of the target surface from the frequency of the beat signal. As stated above, the frequency of the beat signal is determined by the absolute value of the difference between the reference and Doppler shifted beams, so PDV does not respond differently to forward or backward motion of the target plate and can only sense normal motion.

### B. Combined normal and transverse displacement interferometry (NDI/TDI)

The TDI/NDI was developed by Kim *et al.*<sup>10</sup> to monitor the combined normal and transverse displacement motion of a target surface from oblique plate impact experiments. The interferometer utilizes an array of mirrors, beam splitters, and photodiodes along with an optical table in order to manipulate the target and the reference beams. The system makes use of two m-th order diffraction beams from a holographic grating on the surface of the target. A schematic of the conventional combined NDI/TDI is shown in Fig. 2. The diagnostics related to transverse displacements is a result of intensity variations caused by the superposition of the two symmetric  $\pm m$  order diffraction laser beams making an angle  $\theta_m$  with the incident beam, satisfying the equation

$$d \sin \theta_m = m \lambda, \quad (4)$$

where  $d$  is the pitch of the grating, and  $m$  is the order of the diffracted beams.<sup>10</sup>

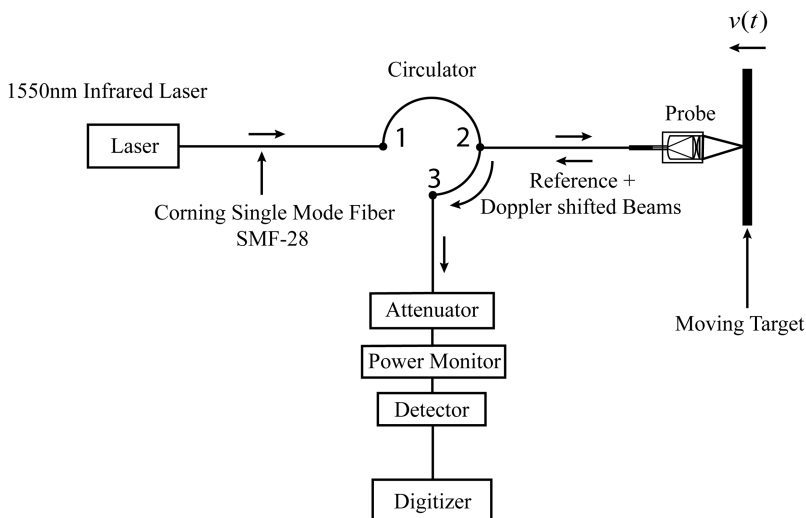


FIG. 1. Shows a schematic of the original fiber-optics based Photonic Doppler Velocimeter (PDV) developed by Strand *et al.* In this configuration, the fiber-coupled probe is used to deliver a reference beam to a moving target and also capture the Doppler shifted beam reflected from the rear surface of the target. The Doppler shifted beam is combined with a reference beam which is provided by back reflection from the rear surface of the probe and creates a beat frequency.

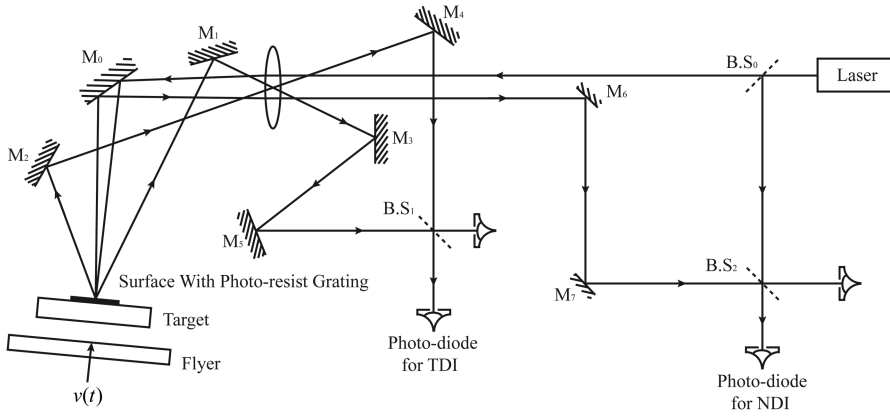


FIG. 2. Shows a schematic of the conventional transverse displacement interferometer developed by Kim *et al.*<sup>10</sup> Here a pair of  $m$ -th order diffracted beams generated from a holographic grating fabricated on the surface of the target plate are combined to create a beat frequency.

The electric field associated with the two  $\pm m$  order diffraction laser beams reflected from a moving target surface can be represented as

$$E_m^+(\theta_m, t) = A_m^+ [\exp\{i(kv_n(t)(1 + \cos\theta_m) + kv_t(t)\sin\theta_m - \omega t - \varphi_o^+)\}], \quad (5)$$

$$E_m^-(\theta_m, t) = A_m^- [\exp\{i(kv_n(t)(1 + \cos\theta_m) - kv_t(t)\sin\theta_m - \omega t - \varphi_o^-\}], \quad (6)$$

where  $k$  is the wave number of the laser light being used,  $\omega$  is the wave frequency, and  $v_n(t)$  and  $v_t(t)$  represent the normal and transverse components of motion, respectively. The time dependent intensity to which a detector responds to the superimposed beam is given by

$$I(t) = I^+ + I^- + 2\sqrt{I^+I^-}\cos\beta\cos\varphi(t), \quad (7)$$

where  $\beta$  is a constant angle between the direction of polarizations of the beams and  $\varphi(t)$  is the time dependent phase difference. Given that the phase change of the beams caused by the components of motion is symmetric, the absolute difference in phase between the two diffracted beams can be expressed as

$$|\Delta\varphi(t)| = 2kv_t(t)\sin\theta_m. \quad (8)$$

Using Eqs. (4) and (8), the transverse displacement per fringe can be expressed as

$$\frac{v_t(t)}{F(t)} = \frac{d}{2m}, \quad (9)$$

where  $F(t)$  refers to the number of fringes. Equation (9) can then be used to determine the complete transverse displacement history of the target free surface under oblique plate impact loading conditions.

### III. DESIGN AND IMPLEMENTATION OF THE ALL-FIBER-OPTICS HETERODYNE COMBINED NDI/TDI

The all fiber-optics NDI/TDI described in the present paper incorporates the principles from those developed by Strand *et al.*<sup>8</sup> in their original PDV design and those developed by Kim *et al.*<sup>10</sup> in the conventional NDI/TDI. This implementation is shown schematically in Figure 3; shown in blue is the channel for the normal motion diagnostics and in red is the channel representing the transverse motion diagnostics. The various optical components of the system are described in Subsections III A and III B on normal displacement motion and the transverse displacement motion.

#### A. Normal displacement motion

In order to monitor the normal component of the particle displacement motion, a beat signal is formed by the superposition of a reference beam from a stationary optical reflector and a Doppler shifted beam reflected from the surface of the target plate. A 2W Erbium fiber coupled laser (IPG Model ELR-2-1550-LP-SF) is used to transport light through a circulator (Thorlabs 6015-3-APC), which allows the passage of

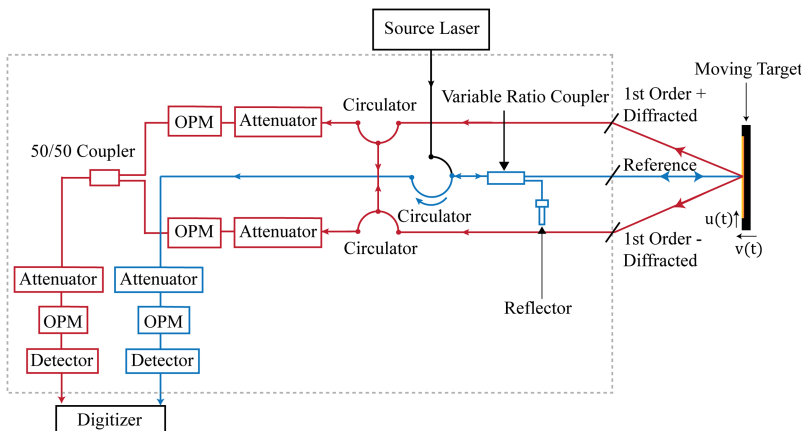


FIG. 3. Schematic of the all fiber-optics combined normal and transverse displacement interferometer system. This design takes advantage of the all-fiber-optics normal displacement interferometer leg (shown in blue) to both deliver the reference beam to rear surface of the target and create first order diffracted beams. These diffracted beams are then captured via fiber coupled collimators and travel through the all-fiber-optics transverse displacement interferometer leg (shown in red) where they are combined to create a beat frequency proportional to the transverse displacement history.

light to and from the target while preventing any back reflection of stray light. The light transported through the circulator is split by a variable ratio coupler (Newport F-CPL-1550-N-FA) to illuminate an optical focuser probe (PM Optics,  $\sim 70\ \mu\text{m}$  beam size,  $\sim 9\ \text{mm}$  working distance) and an optical reflector (EigenLight R-15). The optical probe focuses light to a spot on the target plate and also captures the Doppler shifted light beam reflected from the surface of the target during its normal motion. This Doppler shifted beam is combined with the reference beam to form a beat signal. This phase modulated beam travels through Port 2 of the circulator and out through Port 3, where it is attenuated (Eigenlight IS08-01-15-15) and monitored via an optical power monitor (OPM) model (Eigenlight M520-20XX0-15-15) to ensure that the beam does not exceed the power threshold of the detector (Newport 1554-B). The signal is then sent to a high sampling rate and wide-bandwidth digitizer. Finally, after data manipulation, Eq. (3) is used to determine the normal component of the combined normal and transverse displacement motion of the target plate.

## B. Transverse displacement motion

The transverse component of the displacement motion is monitored by capturing the first order beams, diffracted from a high frequency holographic diffraction grating fabricated on the target free surface, and superimposing the diffracted beams to form a beat frequency. The optical focuser probe, which is illuminated by a 2 W erbium fiber coupled laser, focuses a spot on the grating at the target free surface. The holographic grating diffracts the incoming beam into multiple symmetric higher order beams according to the diffraction law (Eq. (4)). Since first-order beams are of the highest intensity, these are captured and collimated into fibers using two fiber optic collimators (PM Optics,  $\sim 240\ \mu\text{m}$  beam size,  $\sim 20\ \text{mm}$  working distance). Symmetrically diffracted beams from the collimator travel through a pair of circulators which share a port. This allows for the individual beams to be combined via a fiber coupler without creating any backwards reflection, which could result in loss of contrast as well as generation of ghost fringes due to multiple beam reflections in the optical fibers. The beams are combined using a 50/50 coupler (OZ optics FUSED-12-1550-9/125-50/50-3A3A3A-1-1) and form a beat signal which can be attenuated and then detected. The frequency of the beat signal here is directly related to the transverse component of the motion of the target by half of the pitch of the reflective grating. This signal is then stored and monitored with a digitizer and later analyzed to determine the transverse motion. Finally, after signal processing, Eq. (9) can be used to determine the transverse component of particle velocity of a point on the target surface from the digitized fringe data.

## IV. SYSTEM SPECIFICATIONS AND LIMITATIONS

In the implementation of the all-fiber-optics NDI/TDI interferometer, a continuous 1550 nm wavelength infrared laser is utilized. The line widths of the infra-red laser are as narrow as 50 kHz, which corresponds to a coherence length of 6000 m. The other critical optical component is a three-port

circulator, which has a high efficiency (0.85) for transporting light from Port 1 to Port 2 and Port 2 to Port 3, while a very low efficiency ( $<10^{-6}$ ) for transporting light in any other direction.<sup>8</sup> By using single-mode optical fibers (Corning SMF-28), the system described here is a complete fiber-coupled design without any air-transport of the laser beam, except from the fiber-optic probe to the target surface. These components are connected by the FC/APC (fiber channel/angled physical contact) or FC/UPC (fiber channel/ultra-polished physical contact) connectors, which give low back-reflection and insertion loss, so that the overall efficiency of the system is high. The input power from laser is limited by the maximum power limit of the circulators at about 0.5 W. For the experiments conducted in the present study, a laser power of  $\sim 0.3\ \text{W}$  is used to avoid overdriving the circulators. To improve the signal to noise ratio of the transverse displacement fringes, we utilize an external digital DC amplifier to provide approximately  $25\ \mu\text{W}$  of light power at the detector, which results in fringes with  $\sim 160\ \text{mV}$  amplitude at the digitizer. For the case of the normal displacement interferometer, the variable ratio coupler is optimized to yield a high fringe signal to noise ratio without exceeding the saturation limit of the detectors, i.e.,  $700\ \mu\text{W}$ .

The Tektronix DPO70404C digitizer used in the present experiments has an ultra-wide bandwidth of 4 GHz with a record length of 1.25 ms at 25 GS/s sampling rate. Moreover, the maximum particle velocity that can be measured by each individual channel in this system is limited by the combined bandwidth of the 12 GHz detector (with built in amplification) and 4 GHz digitizer used in the system, resulting in an equivalent transmission bandwidth of 3.795 GHz, which corresponds to  $\sim 2900\ \text{m/s}$  measurable particle velocity limit for normal motion diagnostics, and  $\sim 3800\ \text{m/s}$  for transverse motion diagnostics.<sup>8</sup> Digitizing a 3.795 GHz signal of a moving target at 2900 m/s in the normal direction, or 3800 m/s in the transverse direction, and sampling at 25 GS/s provides over 6 data points per fringe, which is sufficient to carry out the data analysis to obtain the free surface displacement versus time history with the desired accuracy.

## V. PROOF OF PRINCIPLE EXPERIMENTS

To demonstrate the working capabilities of the all-fiber-optic NDI/TDI diagnostic system, a series of two symmetric oblique plate-impact experiments are conducted using the 82.5 mm bore single-stage gas gun<sup>21-26</sup> at the Case Western Reserve University. The schematic of the experimental configuration is shown in Fig. 4. This configuration, which is a modification of the experiments conducted previously for studying dynamic frictional slip resistance of metals,<sup>11,27-29</sup> involves the oblique impact of a flyer plate, carried by a sabot and accelerated with compressed nitrogen gas, with a stationary target plate. The two impacting plates are flat and parallel and inclined at an angle of  $22^\circ$  relative to the direction of approach. The impact is made to occur in the target chamber evacuated to a pressure of less than 100 mTorr. The inclination of the flyer and target plates ensures the generation of both the normal and transverse components of particle motion at the rear (free) surface of the target plate. This motion is monitored using all-fiber-optics

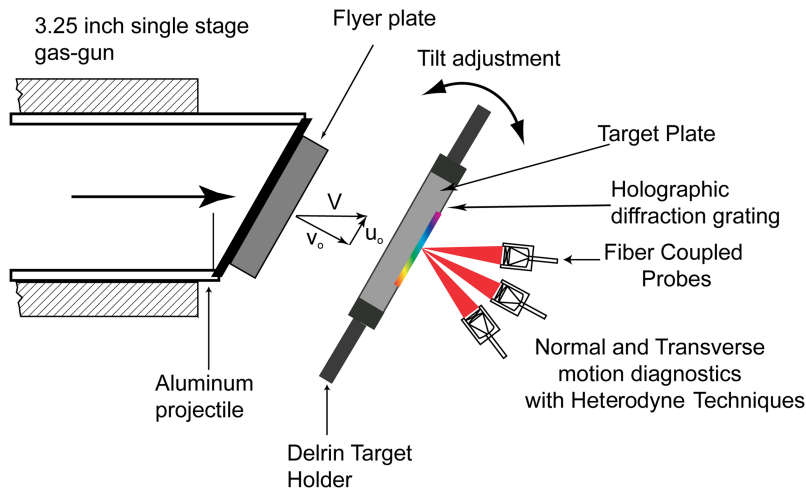


FIG. 4. Schematic of the symmetric oblique plate impact experimental configuration used in the present study.

TABLE I. Selected physical, mechanical, and thermal properties of annealed (as received) AISI H13 tool steel.

Material	Density (Kg/m <sup>3</sup> )	Elastic modulus (GPa)	Compressive strength (GPa)	Shear modulus (GPa)	Longitudinal wave speed (m/s)	Shear wave speed (m/s)
AISI H13 tool steel (annealed)	7760	215	0.75	84	6025	3290

NDI/TDI diagnostic interferometer; it should be noted that an additional amplifier (Stanford Research SR445A Quad 350 MHz RF preamplifier) was utilized for  $5\times$  gain in the transverse motion diagnostic channel prior to recording. This limited the equivalent transmission bandwidth of the transverse motion diagnostics channel to 349 MHz, which corresponds to  $\sim 349$  m/s measurable transverse particle velocity limit. The measured displacement versus time history can be time-differentiated to yield the particle velocity versus time profile using an in-house developed data analysis program in conjunction with the commercial package MATLAB.

In the two symmetric oblique plate impact experiments reported in the present study, the impact velocity of the flyer plate is controlled to be approximately 69 m/s and 126 m/s, while the skew angle is maintained at  $22^\circ$ . The flyer and target plates are flat disks with diameters of 76.2 mm and 41.3 mm, respectively, and are machined from a 76 mm diameter annealed H13 tool-steel rod. Selected physical and mechanical properties of annealed H13 tool-steel are provided in Table I.

To ensure the generation of plane-waves with a wave front parallel to the impact interface, both sides of the flyer and target disks were ground flat to within  $12\ \mu\text{m}$  and then lapped to within 2-3 Newton's rings across the diameter. Lapping is performed on a Lapmaster 15 machine using  $15\ \mu\text{m}$  alumina powder in mineral oil. Moreover, the flyer and target plates are aligned to a parallelism of within  $5 \times 10^{-4}$  rad, using a precision optical prism in conjunction with an auto-collimator.<sup>30,31</sup> A 500 lines/mm holographic diffraction grating is fabricated on the rear surface of target plate via photolithography using Shipley's 1805 series photoresist and CD-26 developer; the grating enables generation of first order diffracted beams at

$\sim 50.8^\circ$ , which are used for transverse motion diagnostics. All measurements of the normal and transverse components of particle velocity at the rear surface of the target plate are made before the arrival of the unloading waves from the lateral boundaries at the monitoring point. In view of this, and during the time interval of interest, the impacting plates can be considered to be essentially infinite in their spatial dimensions.

To estimate the arrival times of the longitudinal, transverse, and the unloading waves (generated during impact), at the monitoring point on the free surface of the target plate, a time versus distance diagram for elastic wave propagation in both the flyer and the target plates is used; the diagram is shown schematically in Figure 5. The elastic longitudinal wave arrives at the free surface of the H13 tool-steel target plate at approximately  $1\ \mu\text{s}$  after impact and is followed by the transverse wave at  $\sim 1.82\ \mu\text{s}$ . The unloading waves from the lateral boundary of the target plate arrive at the monitoring point at  $\sim 3\ \mu\text{s}$ . The arrival times of these waves allow for a window time of  $\sim 2\ \mu\text{s}$  for recording the longitudinal motion and  $\sim 1.16\ \mu\text{s}$  for recording transverse motion.

## VI. RESULTS AND DISCUSSION

Figure 6 shows the raw digitized fringes corresponding to the normal and transverse particle displacement motion of the free surface of the target plate measured by using the newly implemented all-fiber-optics-based NDI/TDI. The experiment was conducted at an impact velocity of 69 m/s, which is just over the limit for fully elastic response of the annealed H13 tool-steel. The solid black line shows the fringe record corresponding to the recorded normal particle displacement motion,

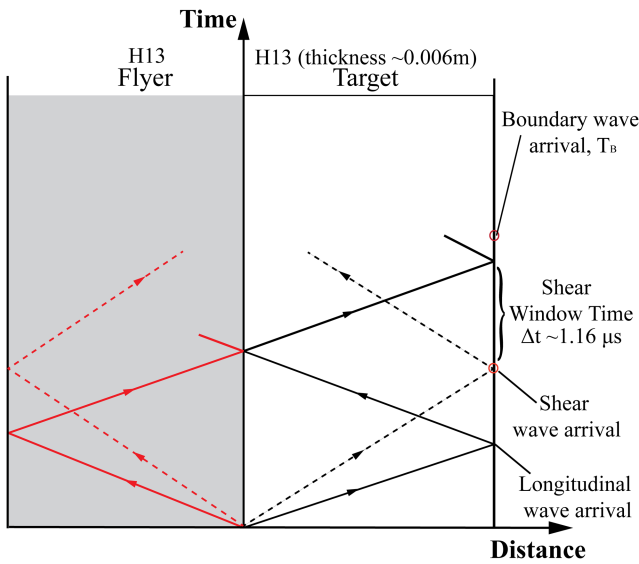


FIG. 5. Time versus distance diagram showing wave propagation in the flyer and target plates as a result of symmetric oblique plate impact assuming perfectly an elastic material behavior.

while the data in red show fringe data corresponding to the transverse component of the particle displacement history.

At the arrival of the longitudinal wave, which occurs at  $\sim 1.016 \mu\text{s}$ , the beat signal variations in the normal particle displacement channel correspond to the normal motion of the free surface of the target. After the arrival of the longitudinal wave, a slowly varying region can be seen in the transverse displacement fringe record, which corresponds to a relatively low transverse motion caused by flyer-target plate misalignment (tilt) at impact; this also demonstrates the insensitivity of the transverse motion diagnostics to normal motion. Only at the arrival of the transverse wave, which occurs at  $\sim 1.838 \mu\text{s}$ , high frequency beat variations are observed in the transverse displacement fringe record. These fast beat frequency

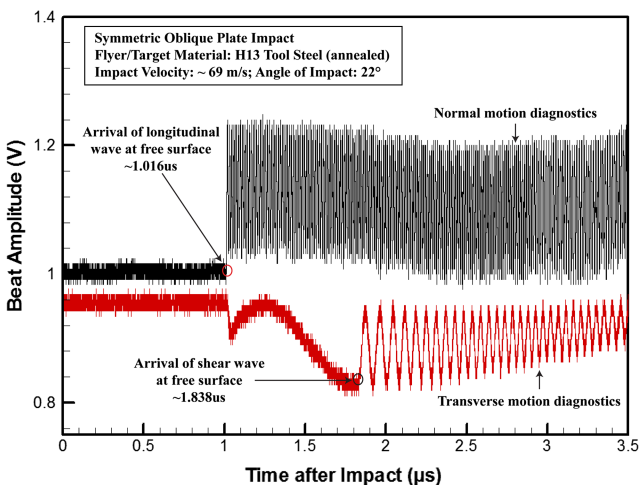


FIG. 6. Shows the beat signal variation at the arrival of the longitudinal and shear waves at the free surface of the target plate monitored via the new implemented all-fiber-optics heterodyne combined NDI/TDI. The figure shows that the all-fiber-optics transverse displacement diagnostics is insensitive to normal motion, as seen by the slowly varying region in the all-fiber-optics transverse displacement fringe signal before the arrival of the shear wave at the target free surface.

variations are sustained throughout the entire time window (duration) of the experiment, which corresponds to a normal motion of  $\sim 200 \mu\text{m}$  of the target surface.

It is to be noted that the beat frequency variation in the normal displacement fringe record is much greater than for the transverse displacements fringe record; this is to be expected since the beat frequency due to the normal displacement interferometer is a factor of  $d/\lambda \sim 29\%$  greater than that for the transverse displacement interferometer for the same particle velocity, and because for this particular experiment, the normal component of the particle velocity is  $\sim 92.7\%$  of the sabot velocity while the transverse component is only  $\sim 37.5\%$ . Also, as observed in Figure 6, the fringe contrast (i.e., amplitude) of the transverse displacement fringes attenuates with time; this attenuation can be attributed to the limited depth of field of the dispensable fiber-optics probes used in the present experiments. From the fringe data, a maximum measurement depth of field can be estimated as  $\sim 350 \mu\text{m}$ , which is the product of the longitudinal particle velocity (65 m/s) and the time from the arrival of the longitudinal wave at the target free surface to where the signal amplitude is unrecognizable from noise ( $5.385 \mu\text{s}$ ).

Figures 7 and 8 show the normal and transverse components of the free-surface particle-velocity versus time profiles measured on the rear surface of the target plate for the two symmetric oblique ( $22^\circ$ ) plate impact experiments conducted in the present study. In both experiments, annealed H13 tool steel was utilized for the flyer and target plates. The impact velocity of the experiment shown in Fig. 7 was 69 m/s while for the one shown in Fig. 8 was 126 m/s. Under these impact conditions, in both experiments, the annealed H13 tool-steel flyer and target plates are expected to become elastic-plastic during impact. The longitudinal and transverse wave fronts are observed to arrive at the target free surface at  $1.016 \mu\text{s}$  and  $1.838 \mu\text{s}$ , respectively, for experiment Shot 1 and at  $0.95 \mu\text{s}$  and  $1.87 \mu\text{s}$  in experiment Shot 2. The dashed lines show the expected normal and transverse particle velocity levels assuming that both the H13 tool-steel flyer and target plates remain perfectly

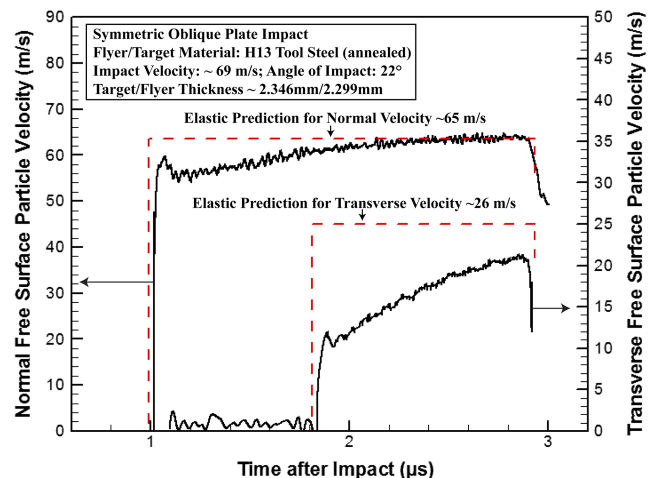


FIG. 7. Normal and transverse components of the free surface particle velocity measured at the free surface (rear) of the target plate using the all-fiber-optics combined NDI/TDI diagnostic system for the symmetric oblique plate impact experiment conducted at 69 m/s impact velocity.

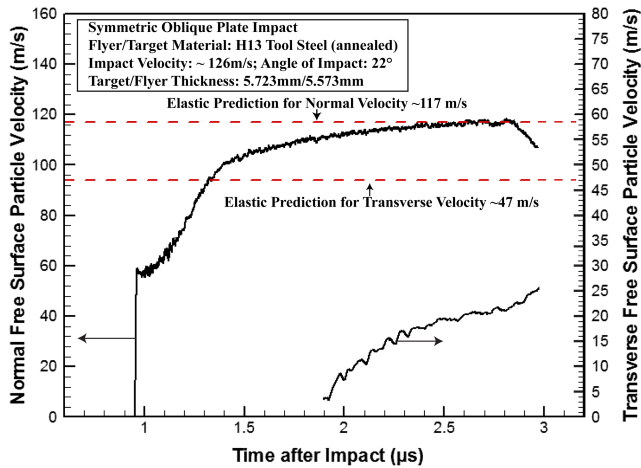


FIG. 8. Normal and transverse components of the free surface particle velocity measured at the free surface (rear) of the target plate using the all-fiber-optics combined NDI/TDI diagnostic system for the symmetric oblique plate impact experiment conducted at 126 m/s impact velocity.

elastic during impact; these are 65 m/s and 26 m/s, respectively, for Shot 1, and 117 m/s and 47 m/s, respectively, for Shot 2. In both experiments, the measured normal particle velocity profiles are observed to approach their respective elastic prediction levels during the window time of the experiments. Moreover, the normal particle velocity profiles show a distinct knee at approximately 58 m/s. This knee in particle velocity profile corresponds to a stress level of 1.35 GPa and represents the dynamic strength of annealed H13 tool steel under the applied multiaxial combined pressure and shear loading conditions. In both experiments, the transverse waves trail the longitudinal wave front in the target. Since the H13 tool-steel target is in its elastic-plastic state, these trailing transverse waves essentially probe the elastic-plastic state of the shocked material. As expected, the amplitude of the transverse wave at the wave front is higher for the case of the lower impact velocity (69 m/s) experiment when compared to the amplitude in the higher impact velocity experiment (126 m/s) because of the much higher levels of inelasticity present in the H13 tool-steel target in the higher impact velocity experiment. Also, from the transverse particle velocity profiles, considerable shear strain hardening can be observed.

## VII. SUMMARY

In the present study, a compact fiber-optics-based heterodyne combined NDI/TDI is developed to monitor combined normal and transverse particle motion in shock wave experiments. This diagnostic tool utilizes similar principles to those of the conventional PDV and transverse displacement interferometer to capture symmetric diffracted beams from a holographic grating at the target surface and deliver them past circulators where they are combined to form distinguishable beat frequency variations. Similar to the PDV, this new fiber-optic-based combined NDI/TDI system has many of the

advantages of both the traditional NDI/TDI and VISAR, while avoiding major disadvantages of the individual systems such as cost, maintenance, and size. The limiting bandwidth of this all-fiber-optics heterodyne combined NDI/TDI system is 3.795 GHz, which corresponds to a maximum measurable velocity of 2900 m/s for normal motion and 3800 m/s for transverse motion. A series of two proof-of-principle symmetric oblique plate impact experiments were performed to demonstrate the feasibility of this newly implemented diagnostic tool in the measurement of combined normal and transverse displacement motion.

## ACKNOWLEDGMENTS

The authors would like to acknowledge the financial support of the U.S. Department of Energy through the Stewardship Science Academic Alliance (Grant Nos. DE-NA0001989 and DE-NA0002919) in conducting the present research.

- <sup>1</sup>L. M. Barker and R. E. Hollenbach, *Rev. Sci. Instrum.* **36**, 1617 (1965).
- <sup>2</sup>L. M. Barker and R. E. Hollenbach, *J. Appl. Phys.* **41**, 4208 (1970).
- <sup>3</sup>D. T. Casem, S. E. Grunschel, and B. E. Schuster, *Exp. Mech.* **52**, 173 (2012).
- <sup>4</sup>M. Mello, V. Prakash, and R. J. Clifton, "Shock compression of condensed matter," in Proceedings of the American Physical Society Topical Conference, 1991.
- <sup>5</sup>V. Prakash and R. J. Clifton, in Proceedings of the 22nd National Symposium on Fracture Mechanics : ASTM Special Technical Publication 1131, 1992.
- <sup>6</sup>L. M. Barker and R. E. Hollenbach, *J. Appl. Phys.* **43**, 4669 (1972).
- <sup>7</sup>W. C. Sweatt, P. L. Stanton, and J. O. B. Crump, *Proc. SPIE* **1346**, 151 (1991).
- <sup>8</sup>O. Strand, D. Goosman, C. Martinez, T. Whitworth, and W. Kuhlow, *Rev. Sci. Instrum.* **77**, 083108 (2006).
- <sup>9</sup>C. Avinadav, Y. Ashuach, and R. Kreif, *Rev. Sci. Instrum.* **82**, 073908 (2011).
- <sup>10</sup>K. S. Kim, R. J. Clifton, and P. Kumar, *J. Appl. Phys.* **48**, 4132 (1977).
- <sup>11</sup>F. Yuan and V. Prakash, *J. Mech. Phys. Solids* **56**, 542 (2008).
- <sup>12</sup>L. C. Chhabildas, *Proc. SPIE* **0427**, 136 (1984).
- <sup>13</sup>L. Chhabildas, H. Sutherland, and J. Asay, *J. Appl. Phys.* **50**, 5196 (1979).
- <sup>14</sup>F. Yuan, V. Prakash, and J. J. Lewandowski, *Mech. Mater.* **42**, 248 (2010).
- <sup>15</sup>F. Yuan and V. Prakash, *Tectonophysics* **558–559**, 58 (2012).
- <sup>16</sup>D. Dolan, *Rev. Sci. Instrum.* **81**, 053905 (2010).
- <sup>17</sup>X. Wu, W. Xia, X. Wang, H. Song, and C. Huang, *Meas. Sci. Technol.* **25**, 055207 (2014).
- <sup>18</sup>E. A. Moro, *J. Phys.: Conf. Ser.* **500**, 142023 (2014).
- <sup>19</sup>M. I. Kaufman, R. M. Malone, B. C. Frogget, D. L. Esquibel, V. T. Romero, G. A. Lare, B. Briggs, A. J. Iverson, D. K. Frayer, and D. DeVore, *Proc. SPIE* **6676**, 667607 (2007).
- <sup>20</sup>B. Jensen, D. Holtkamp, P. Rigg, and D. Dolan, *J. Appl. Phys.* **101**, 013523 (2007).
- <sup>21</sup>N. S. Liou, M. Okada, and V. Prakash, *J. Mech. Phys. Solids* **52**, 2025 (2004).
- <sup>22</sup>F. Yuan, L. Tsai, V. Prakash, A. Rajendran, and D. Dandekar, *Int. J. Solids Struct.* **44**, 7731 (2007).
- <sup>23</sup>F. Yuan, V. Prakash, and J. J. Lewandowski, *J. Mater. Res.* **22**, 402 (2007).
- <sup>24</sup>M. Shazly and V. Prakash, *J. Appl. Phys.* **104**, 083513 (2008).
- <sup>25</sup>L. Tsai and V. Prakash, *Int. J. Solids Struct.* **42**, 727 (2005).
- <sup>26</sup>G. Sunny, F. Yuan, V. Prakash, and J. J. Lewandowski, *J. Appl. Phys.* **104**, 093522 (2008).
- <sup>27</sup>F. Yuan, N.-S. Liou, and V. Prakash, *Int. J. Plast.* **25**, 612 (2009).
- <sup>28</sup>R. J. Clifton and K. J. Fruttsch, *J. Tribol.* **119**, 590 (1997).
- <sup>29</sup>V. Prakash and F. Yuan, *Trans., Am. Geophys. Union* **85**, 435 (2004).
- <sup>30</sup>P. Kumar and R. Clifton, *J. Appl. Phys.* **48**, 1366 (1977).
- <sup>31</sup>V. Prakash, *Tribol. Trans.* **41**, 189 (1998).